nature communications

Article

https://doi.org/10.1038/s41467-026-68569-z

Global alluvial channel patterns

Received: 29 July 2024

Accepted: 9 January 2026

Published online: 21 January 2026

Check for updates

Qiuqi Luo[1,2,3], Edward Park[4,5,6] ✉, Edgardo M. Latrubesse[7], Xuehui Pi[8], Hongwei Fang[1], Yan Liu[1], Adam D. Switzer[5], Dongfeng Li[9], Wenhui Qiu[1], Chunmiao Zheng[1,10], Pan Liu[11] & Lian Feng[3] ✉

Quantitative analysis of alluvial channel patterns is essential in fluvial science, as their morphology both reflects and influences river behavior through interactions with water and sediment regimes, landscape processes, and human interventions. However, a comprehensive global study to identify predominant channel patterns and their underlying mechanisms remains lacking. Here, we map global alluvial channel patterns using high-resolution satellite observations. Our results reveal a hidden dominance of anabranching channels that surprisingly constitute half (51%) of total reach length globally, exceeding meandering (24%), straight (18%), and braided (7%) channels. In non-mountainous settings, anabranching channels dominate most continents except Oceania. They are not confined to typical alluvial lowland systems, also comprising 50% of alluvial tracts in mountains. While anabranching is typically associated with gentle slopes and expansive floodplains, these conditions are not exclusive determinants. The prevalence of anabranching channels transforms fundamental perspectives on global river systems, posing challenges for the fluvial geomorphology community.

Fluvial geomorphology is a cornerstone of Earth system science that reveals insights into the complex processes that govern river dynamics[1,2], landscape evolution[3], and the multifaceted interactions between the hydrophysical functioning of rivers and human activities, ecosystems, and natural disasters[4,5]. Since the discipline's early days, researchers have classified the morphological diversity of river systems by identifying distinct styles of alluvial channel patterns[6–8]. Traditionally, four primary alluvial channel patterns have been recognized in fluvial studies worldwide: straight, meandering, braided, and anastomosing[9,10]. This four end-member classification has served as a baseline for shaping our understanding of river processes since the late 1970s, and is commonly applied to interpret the fluvial geological record and the role of fluvial systems through Earth's history[8,10,11].

Anabranching channels, another multichannel pattern, were proposed through pioneering studies of inland Australian rivers[12–14]. Anabranching rivers are characterized by a network of interconnected channels separated by stable vegetated alluvial islands that preserve their hydraulic and morphological identity even at bankfull stages[1,12,15]. Some studies have further restricted the term "anastomosing" to a specific subset of relatively distinctive low-energy anabranching systems, typically associated with fine-grained or organic vertical accretion deposition[12,16–19]. Thus, anastomosing channels are part of the anabranching family, and the full extent of anabranching channel systems is much broader. Until recently, anabranching rivers were regarded as relative rarities and, consequently, received limited attention in the development of fluvial geomorphology theories[20,21].

[1]School of Environmental Science and Engineering, Southern University of Science and Technology, Shenzhen, China. [2]Aerospace Information Research Institute, Henan Academy of Sciences, Zhengzhou, China. [3]State Key Laboratory of Information Engineering in Surveying, Mapping and Remote Sensing, Wuhan University, Wuhan, China. [4]National Institute of Education, Nanyang Technological University, Singapore, Singapore. [5]Earth Observatory of Singapore and Asian School of the Environment, Nanyang Technological University, Singapore, Singapore. [6]Center for Climate Change and Environmental Health, Nanyang Technological University, Singapore, Singapore. [7]Graduate Program in Environmental Sciences (CIAMB), Federal University of Goiás-UFG, Campus II, Goiania, GO 74690-900, Brazil. [8]College of Surveying and Geo-Informatics, Tongji University, Shanghai, China. [9]Key Laboratory for Water and Sediment Sciences, Ministry of Education, College of Environmental Sciences and Engineering, Peking University, Beijing, China. [10]School of the Environment and Sustainable Engineering, Eastern Institute of Technology, Ningbo, China. [11]State Key Laboratory of Water Resources Engineering and Management, Wuhan University, Wuhan, China. ✉e-mail: edward.park@nie.edu.sg; lian.feng@whu.edu.cn

However, this perception began to change with the discovery that the top ten largest rivers in the world, with mean discharges exceeding 17,000 $m^3 s^{-1}$ (mega rivers), are dominated by anabranching patterns[22]. A further study revealed that nineteen of the twenty largest rivers by water discharge exhibit anabranching patterns, with only the Mississippi River showing a stronger tendency for meandering, and rivers such as Ob, Ucayali, and Ganges with reaches displaying anabranching sinuous patterns[23]. Thus, it may be inferred that anabranching patterns represent the ultimate planform adjustment for mega rivers and can be considered major and fundamental components of the fluvial system.

Though advancements have been made in anabranching research, the perception that anabranching is less common than single-channel meandering or braiding persists[14], possibly due to the limited scope of previous studies, which often focused on specific case study sites, such as inland Australian rivers[13,24]. Recent advancements in remote sensing technology have enabled the observation of river systems at a global scale[2,25], allowing us to classify river channel patterns, understand their geographic distribution, examine their change through time, and finally re-evaluate the classification of river channel patterns[26–28]. A recent study explored the key variables influencing anabranching, but its focus was on the twenty largest river basins rather than offering a global perspective across different scales[29]. It did not provide quantitative or statistical insights into the distribution of meandering, braided, and straight channels, nor did it assess geomorphological predictors to discriminate anabranching from meandering and braided patterns. Another recent effort characterized river channel belts for 2020 using Landsat-8 images[30], finding that the likelihood of river channels being single- versus multi-threaded by surface area was 48 vs 52%, respectively. However, they grouped braided and anabranching channels under the same multi-threaded category, which represents a conceptual error in geomorphology. Despite being valuable, due to the absence of a geomorphologically based framework, their study did not provide a proper assessment of channel patterns but rather employed a simplistic two-category classification that conflated distinct channel types, and they did not differentiate between alluvial and rocky channels, resulting in the flawed grouping and counting of them together with alluvial channels. In addition, they relied on pixel-based predictions instead of reach-based estimates, resulting in the simultaneous representation of single- and multi-threaded types within the same cross-section. These methodological limitations underscore the pressing need for a thorough and explicit study on global alluvial channel patterns. Despite this recognized need, a systematic global study was yet to be conducted to determine the dominant fluvial patterns on Earth.

Here, to address these knowledge gaps, we map the entire population of alluvial channels and present a comprehensive global analysis, detailing the geographic distribution of various channel patterns and assessing their quantitative representativeness across major climatic-physiographic zones and continents. We uncover the distribution and dominance of anabranching rivers, challenging the long-standing view that anabranching rivers are anomalies. Instead, we propose that they are not only globally widespread but also the dominant alluvial channel pattern worldwide. We further assess potential factors driving the prevalence of different alluvial channel patterns in non-mountainous regions. Based on our findings, we advocate for reshaping foundational concepts in fluvial geomorphology to support the development of future river conservation, restoration, and management strategies essential for the sustainable management of river systems on a global scale.

Results

Establishment of a global alluvial channel pattern (GACP) dataset

Here, we present the global alluvial channel pattern (GACP) dataset, a queryable, global-scale dataset that delineates the spatial distribution of alluvial river channel types. The GACP distinguishes four major channel types—anabranching, braided, meandering, and straight—by integrating two state-of-the-art datasets: the Global Surface Water Occurrence (GSWO)[31] dataset and the Surface Water and Ocean Topography River Database (SWORD)[32]. The GSWO dataset, derived from 30 m resolution Landsat satellite observations spanning 1984 to 2020, provides long-term estimates of water occurrence probabilities. SWORD serves as the primary global hydrography reference, with each river reach averaging approximately 10 km in length. Channel pattern classification was performed using a hierarchical algorithm with quadruple control, based on key morphology and hydrological attributes, including channel branching degree (Islands and Bars Index, IBI), the ratio of islands/bars area to total channel area, sinuosity, and the vegetation and inundation characteristics of in-channel features ("Methods" and Supplementary Figs. 1–4). Validation against high-resolution images from Google Earth confirms the reliability of our classification approach, with an overall accuracy exceeding 88% (Supplementary Fig. 5 and Supplementary Table 1).

We exclude reaches flowing over bedrock (see "Methods") or narrower than 150 m (Supplementary Note 1). In addition, very dry rivers with extremely low water occurrence over the past four decades —those with water occurrence rarely exceeding 25%, equivalent to less than one season of inundation per year based on the available historical series[31]—were removed from the analysis. Following these exclusions, we categorized the remaining alluvial reaches into three physiographical regions: non-mountainous reaches, mountainous landscapes, and coastal reaches. Coastal reaches are defined as areas within 25 km of the coastline[33] or within deltas[34], with an elevation below 100 m; mountainous alluvial reaches are identified as regions that fall within a 1 km buffer of mountainous areas[35,36] and overlap with the drainage network and unconsolidated sediment zones[37]; and the remaining areas are classified as non-mountainous alluvial reaches (see "Methods"). Rivers flowing through mountain valleys or bedrock are often geologically confined and store a small proportion of fluvial deposits, which dilutes the importance of the alluvial channel-floodplain fractions, while coastal reaches affected by waves or tides are subject to particular hydro-geomorphological processes, and non-mountainous alluvial river reaches are those unaffected by coastal processes (i.e., tides and waves) and ideally not confined by geology (i.e., geologic lateral constraints or bedrock). Notably, our study focuses on non-mountainous alluvial rivers, including those in lowlands, low dissected terrains, plateaus, and highlands. For example, into this category were included alluvial reaches of rivers draining old terrains (shields and plateaus), such as the cratonic areas of South America and large parts of Central and Southern Africa. With the classification algorithm applied to the selected reaches from SWORD, we analyzed alluvial channel pattern predominance and distribution at multiple spatial scales, including the global level, physiographical regions, physio-climate zones, continents, and river basins.

Global channel patterns and the dominance of anabranching

The total length of alluvial channel reaches investigated in our GACP datasets is 0.69 million km, with individual reaches ranging from 0.3 to 38 km, covering 38% of alluvial reaches in the SWORD dataset (Supplementary Fig. 1). Our GACP results at a global scale suggest that multi-threaded channels (anabranching) account for 51% (0.35 million km) of the total reach length, while single-threaded channels (braided, meandering, and straight) constitute the remaining 49% (Fig. 1). Specifically, anabranching channels emerge as the predominant pattern, braided channels account for 7%, meandering channels represent an additional 24%, and straight channels constitute 18%. Notably, 5% of global channels occur in axial river reaches, where straight channels are connected to two or more anabranching or meandering morphological structures (Supplementary Fig. 6).

https://doi.org/10.1038/s41467-026-68569-z

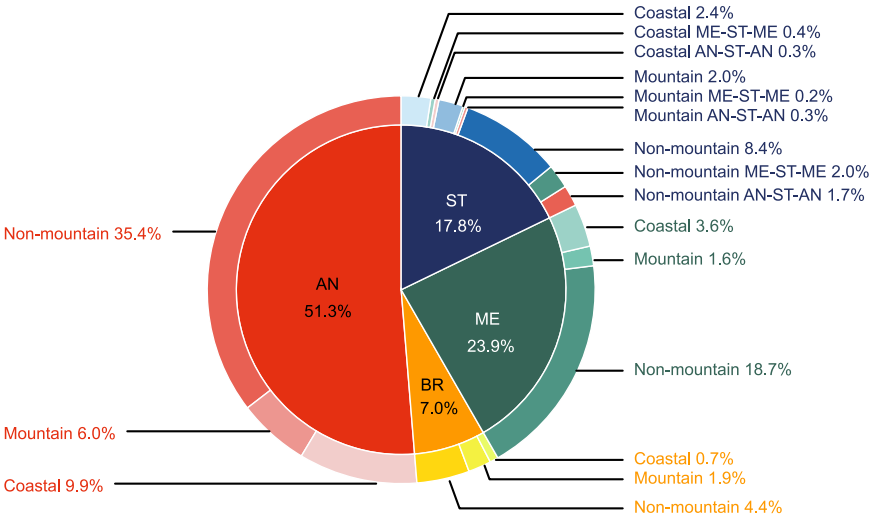

Fig. 1 | The proportion of global alluvial channel patterns. The length proportion of four channel types in different regions (i.e., non-mountain, mountain, and coastal) are shown using pie charts. AN anabranching, BR braided, ME meandering, ST straight. AN-ST-AN: the straight channel is connected to two or more anabranching channels, ME-ST-ME: the straight channel is connected to two or more meandering channels. Coastal reaches are defined as regions within 25 km of the coastline[33] or within deltas[34], with elevation less than 100 m. Mountainous reaches are regions intersected by both the 1 km buffer boundaries of the mountain[35,36] and the unconsolidated sediments map[37]. The remaining reaches are classified as non-mountainous reaches, which are not intersected by the 1 km buffer boundaries of the mountain map.

Non-mountains host 71% of our observed global reach length, predominantly featuring anabranching channels (50%), while braided, meandering, and straight channels constitute 6%, 26%, and 17%, respectively (Figs. 2a, c–j). Within the equatorial belt (~10°S–5°N) and cold high-latitude (~50°N–80°N) non-mountainous regions, anabranching and meandering channels are the most prevalent. Approximately 40% of non-mountainous channels are located in cold physio-climatic conditions where multi-threaded channels are more prevalent (56% anabranching in cold non-mountainous channels; Fig. 2b) compared to single-threaded channels (22% meandering, 18% straight, and 4% braided). When examining the distribution of non-mountainous channels by continent, anabranching channels dominate across all continents, except for Oceania (Fig. 2a and Supplementary Tables 1 and 2). However, dry ephemeral anabranching channels in central Australia's desert were not included in the analysis, leading to an underestimation of anabranching in these areas. Anabranching channels are particularly prominent in Africa, accounting for 54% of the river length in African non-mountainous channels—the highest proportion among the six continents—due to their widespread presence across most parts of the Niger, Congo, and Nile River basins (65%, 64%, and 61% of the total length of respective basins in non-mountains) (Fig. 3). Regarding braided channels, Asia holds the highest fraction of non-mountainous braided channels (10% of reach length in Asian non-mountains), predominantly found in upland regions (Supplementary Fig. 13).

Mountain rivers are characteristically confined to rocky, steep valleys with in-channel dominant processes and landforms, and commonly have bedrock channels with non-existent to poorly developed floodplains and conspicuous hillslopes sediment delivery from mass wasting processes[38,39]. Those kinds of mountain rivers are not included in our analysis, and we concentrate our study on alluvial patterns in mountain areas only (see "Methods").

In mountainous environments, which contribute nearly a tenth of our observed global river length, anabranching channels comprise 50%, with braided, meandering, and straight channels representing 16%, 14%, and 21%, respectively (Supplementary Fig. 7a). Anabranching channels are prevalent in alluvial tracts of mountainous regions, and notable examples include the Huallaga and Ene Rivers in the Andes Mountains, Indigirka River in the East Siberian Mountains, as well as Keele and South Nahanni Rivers within the Mackenzie Mountains (Supplementary Fig. 14). Mountainous braided channels are extensively distributed across major ranges, such as the High Mountain Asia, East Siberian Mountains, Alaska Range, and New Zealand's mountainous regions. Meandering channels are also found in alluvial mountain valleys and the influence of peat bogs in periglacial zones. For example, in Tierra del Fuego, Argentina, rivers predominantly show meandering patterns in the post-glacial period, driven by extensive peat bog deposits within large former glacial zones, dictating the fluvial styles (Supplementary Fig. 15e, f)[40]. In coastal regions, which represent 17% of our observed global river length, anabranching channels dominate with 58%, followed by meandering at 21%, straight at 18%, and braided at 4% (Supplementary Fig. 7b). Notably, European coastal channels are distinctively marked by straight patterns, constituting nearly one-third of their lengths, largely due to extensive human channelization[41–43].

In large river basins where rivers exceed a mean annual discharge of 1000 $m^3 s^{-1}$, fifteen of the twenty largest basins exhibit anabranching channel patterns that span at least half of their non-mountainous basin areas. The proportion of anabranching reaches in these basins ranges from a minimum of ~40% (St. Lawrence) to as much as ~74% (Amur), with an average of 57 ± 10% across all observable non-mountainous reaches at their basin scale (Fig. 3). Our findings corroborate previous studies, reinforcing that anabranching channels represent the end-member pattern within large river basins (Supplementary Fig. 5b)[22,29]. Even the Mississippi basin, traditionally regarded as a classic example of meandering river, approximately 44% of its non-mountainous tracts are characterized by anabranching patterns. We highlight the widespread prevalence of anabranching channels not only in large river basins worldwide with tens of thousands of cumecs ($m^3 s^{-1}$) of mean annual discharge, but also across smaller-sized river basins with a few hundred cumecs ($m^3 s^{-1}$). Beyond the 20 large river basins mentioned, we observed that in half of the remaining smaller-sized river basins, anabranching channels constitute over one-third of reach length within their non-mountainous basin areas. The highest fraction of anabranching channels relative to total non-mountainous reach length is found in the Ili River basin, Kazakhstan, where they account for 86% of reach length within its non-mountainous basin areas. This pattern is similarly prominent in other smaller basins, such as the São Francisco and Magdalena basins, where anabranching channels comprise over

https://doi.org/10.1038/s41467-026-68569-z

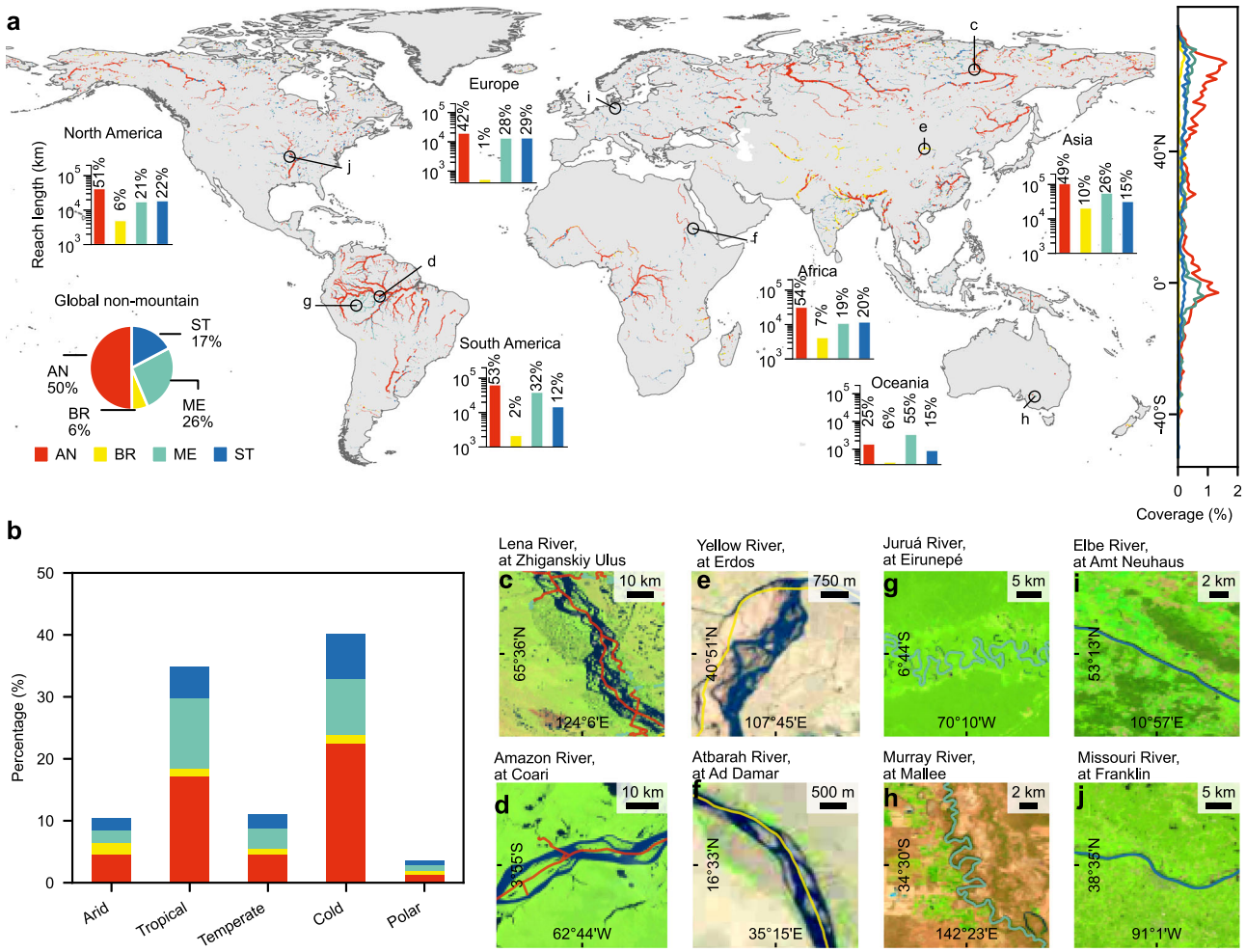

Fig. 2 | The distribution of global non-mountainous alluvial channel patterns. Non-mountainous alluvial channel patterns are mapped on **a**. Latitudinal profiles summarizing (by 1°) the proportion of different channel types (i.e., AN anabranching, BR braided, ME meandering, ST straight) as a percentage of the total non-mountainous reach length are shown on (**a**). The proportions of different channel types using pie charts and bar plots are presented within (**a**). Physioclimatic distribution on four types as a percentage of non-mountainous reach length is visualized on (**b**). Planform characters of the channels are displayed in (**c**–**j**) (anabranching: **c**, **d**; braided: **e**, **f**; meandering: **g**, **h**; straight: **i**, **j**) using Landsat true-color images. Basemaps in (**a**) from Natural Earth (naturalearthdata.com). Map created using Python 3.9.

three-quarters of reach length within their non-mountainous basin areas.

Interestingly, global non-mountainous anabranching channels demonstrate diverse behaviors, with some showcasing tendencies towards braiding, notably in Asia (i.e., the Brahmaputra, Indus, Irrawaddy Rivers), as well as the northwestern South American foreland Andean rivers (i.e., Meta, Napo, Aguarico Rivers). Conversely, other large rivers show anabranching reaches with sinuous-meandering tendencies, such as the Ucayali, Ob, and Ganges Rivers (Supplementary Fig. 17).

Mechanisms underlying anabranching dominance and alluvial channel pattern formation in non-mountainous terrains

To unravel the intricate interplay of hydro-geomorphic factors driving alluvial channel patterns in non-mountains worldwide, we synthetically delved into four classical key variables: water surface slope, unit stream power, average floodplain width to average channel width ratio (FPW/W), and suspended sediment concentrations (Supplementary Note 3).

Rivers can possess identical slopes yet exhibit different channel patterns (Fig. 4a), with these disparities often influenced by the associated discharge (mean annual discharge or bankfull discharge)[22]. Conventionally, slope-discharge plots show a decrease in slope as discharge increases, but they are often inadequate in distinguishing between channel styles, particularly in the context of large rivers[22]. When bankfull discharge is considered, anabranching channels tend to feature shallower slopes than braided channels at similar discharges (Fig. 4e). Specifically, some high-slope (i.e., $>200\,\mathrm{cm\,km^{-1}}$) anabranching rivers, with bankfull discharges between 100 and 500 $\mathrm{m^3\,s^{-1}}$, are often situated in periglacial regions, such as Siberia, Alaska, Scandinavian Peninsula, and Baffin Island where permafrost exerts a substantial interaction on fluvial processes (Supplementary Fig. 16). However, meandering channels, associated with bankfull discharges from 100 to 5000 $\mathrm{m^3\,s^{-1}}$, typically occur in lower slope ranges and exhibit even shallower slopes than anabranching channels, until discharges reach 5000 $\mathrm{m^3\,s^{-1}}$, at which point slopes across different channel types converge.

The unit stream power across different channel types overlaps substantially (Fig. 4b), with half of the braided channels exceeding 25 $\mathrm{W\,m^{-2}}$. In contrast, 84% of the anabranching channels and 93% of the meandering channels have unit stream power below 25 $\mathrm{W\,m^{-2}}$. Anabranching channels with high energy are mainly located in periglacial zones mentioned earlier (i.e., Siberia, Alaska, Scandinavian Peninsula, and Baffin Island), where unique seasonal processes contribute to

https://doi.org/10.1038/s41467-026-68569-z

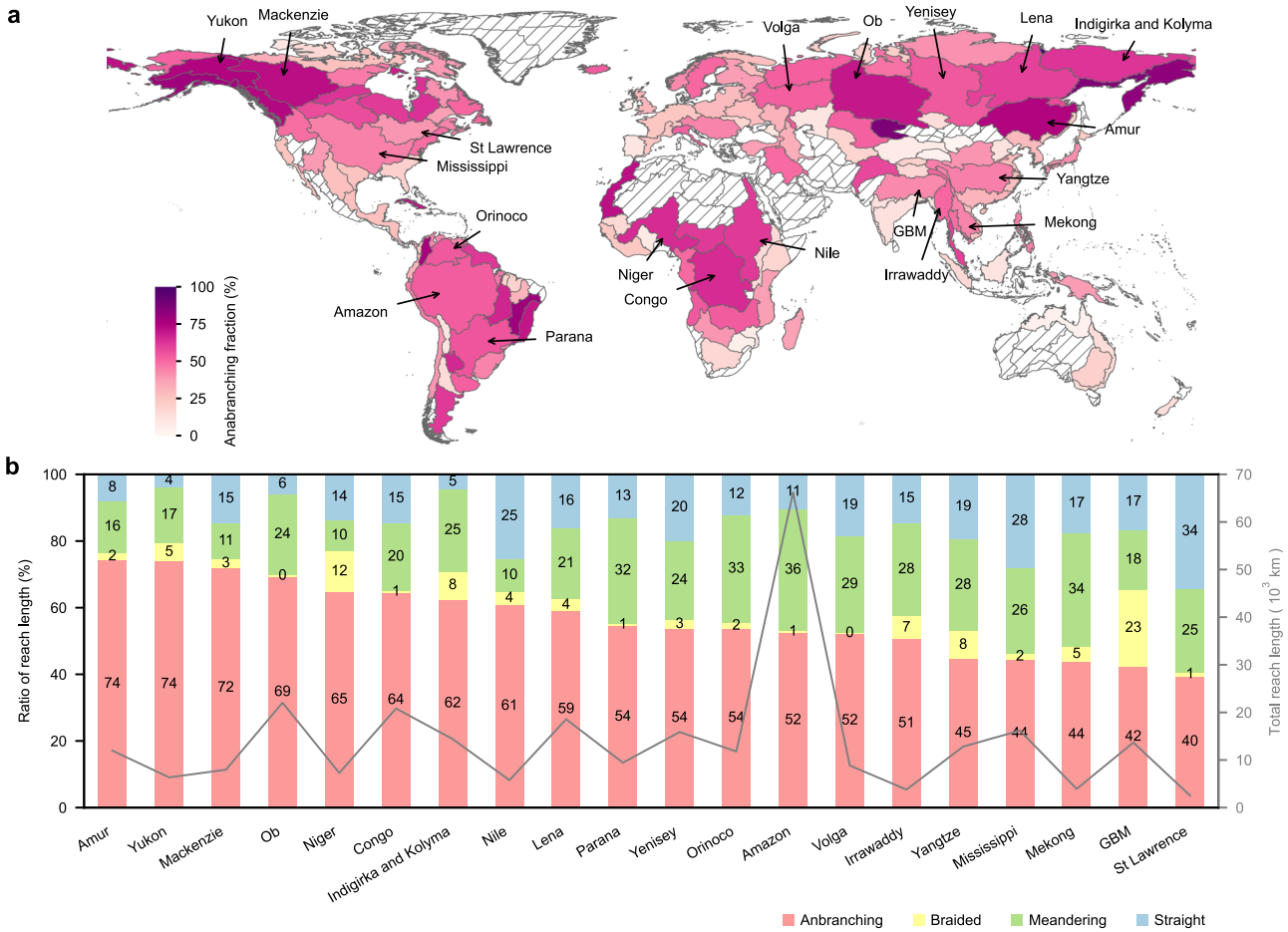

Fig. 3 | Basin-level statistics for non-mountainous alluvial channels. a Fraction of anabranching channels at the basin scale in non-mountainous regions. The locations of the 20 largest river basins with rivers exceeding a mean annual discharge of 1000 $m^3 s^{-1}$ are indicated on the global map. Hatch areas denote basins with no anabranching channels detected in non-mountains. **b** The proportion of four channel types for the 20 largest river basins, sorted in descending order of anabranching fraction. The proportions for each channel type within their non-mountainous basin areas are annotated on their respective bars. The grey line signifies the total reach length within each non-mountainous basin. GBM Ganges-Brahmaputra-Meghna River. The level-3 basin boundaries were provided by HydroBASIN dataset[103]. Basemaps in (**a**) from Natural Earth (naturalearthdata.com). Map created using Python 3.9.

maintaining high energy and enabling the development of anabranching patterns on steeper slopes than those typically observed.

When examining the adimensional parameter FPW/W (Fig. 4c), half of the straight and braided channels have values below 2.1 and 1.8, respectively, suggesting floodplain widths similar to channel widths for these channel types. In contrast, anabranching channels exhibit a wide range of FPW/W values, reflecting considerable variability in floodplain width from narrow to expansive. Meandering channels, on the other hand, show higher average FPW/W values, suggesting that their floodplains may be wider relative to their channel widths due to higher migration rates.

Our global-scale quantification confirms the requirements of high slope and high unit stream power for braided formation, yet it does not directly correlate with high sediment transport rates reported by previous studies[44,45] (Fig. 4a, b, d, e). Suspended sediment concentrations in braided channels are not notably high (~ 200 mg l^{-1}, Fig. 4d), primarily due to the dominance and morphogenetic role of bedload transport[44]. Thus, despite short-lived peaks during floods, suspended sediment may not be noticeably relevant to braided channels. In contrast, meandering channels exhibit a wide range of suspended fine sediment concentrations, from ~10 mg l^{-1} to exceptionally high levels in mountainous rivers, where concentrations can exceed ~15,000 mg l^{-1}. Anabranching channels display a broad range of suspended sediment concentrations as well (see Supplementary Table 4), but overall, suspended sediment concentrations in anabranching rivers are slightly lower than meandering rivers (Fig. 4d).

Employing principal component analysis (PCA) as a trial (Supplementary Note 3), we quantified the combined influence of these variables on non-mountainous alluvial channel patterns (Fig. 4f). Our global results demonstrate that the channel types are not strictly segregated within the PCA space, although braided channels tend to differ substantially from the other three types, showing higher values of slopes, power, and lower FPW/W (Fig. 4a–c). We recognize that categorizing alluvial channel patterns using simple discriminators remains challenging, as rivers with different patterns can exhibit subtle changes in variables, such as discharge or slope (e.g., differences might be as minimal as a few centimeters per kilometer in slope for the same discharge). This complexity is further compounded by regional hydroclimatic and geomorphological contexts, which induce overlap in these variables across diverse channel types, and also because anabranching is a geomorphologically diverse population that spans through a broad range of morphodynamic conditions, from low to high suspended sediment concentrations, low to relatively high unit stream power, and low to high slopes (Fig. 4a–c).

Widespread implications

Our database of global alluvial channel patterns provides a platform for re-evaluating the long-standing view that anabranching rivers are

https://doi.org/10.1038/s41467-026-68569-z

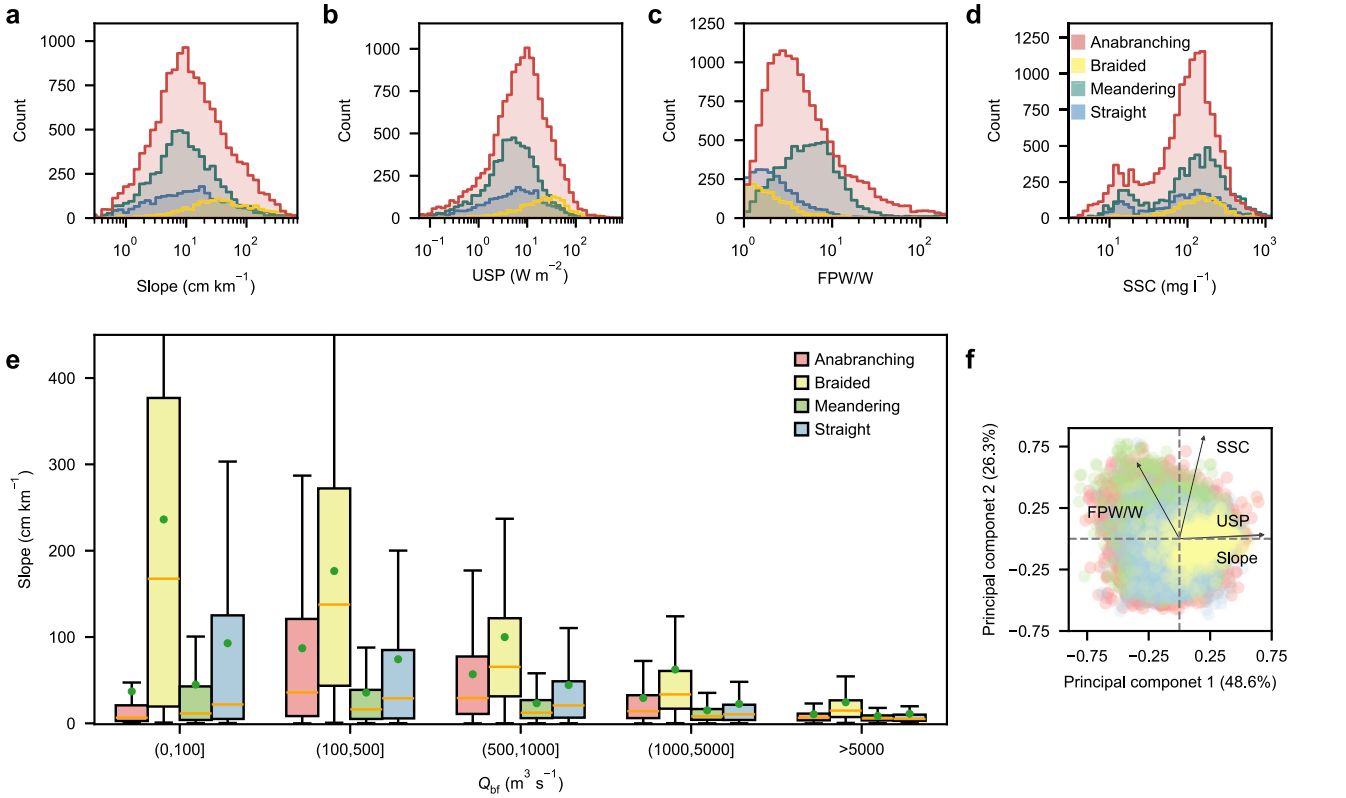

Fig. 4 | Hydro-geomorphic factors driving alluvial channel patterns in non-mountains. The histograms of Slope (water surface slope), USP (Unit stream power), FPW/W (average floodplain width to average channel width ratio), and SSC (suspended sediment concentrations) for four reach types in non-mountains are represented by (**a**–**d**), respectively. **e** Boxplots of slope and bankfull discharge for each reach types. Note that the boxplot edges indicate the first (Q1) and third quartile (Q3) of the data, while the length of whiskers is 1.5 times the IQR (Interquartile range, defined as Q3–Q1), with orange line at the median and green point at the mean. **f** Loading plots of principal component analysis (PCA) based on four explanatory variables. The directions of explanatory variables indicated with black arrows.

less common than meandering or braided rivers. We imply that the widespread physioclimatic and physiographic occurrence, the diversity of anabranching patterns, the scale of the rivers, and their dominance among large rivers position anabranching as the global dominant channel pattern. While fluvial theory has focused for decades on meandering systems and[28,46–50], to a lesser extent, on braided systems, theoretical developments for anabranching have been largely confined to maximum flow efficiency and the least action principle[20,51]. Considering that their distribution is pervasive, with proportions of 50%, 50%, and 58% observed in non-mountainous, mountainous, and coastal regions, respectively, the widespread prevalence of anabranching channels underscores their pivotal role in advancing fluvial geomorphological theories.

As anabranching spans a broad range of morphodynamic conditions, it has been postulated that anabranching systems may develop under both equilibrium and disequilibrium state[21,51,52]. Adding to that, by considering the complex morphologies found in nature, we claim that anabranching channels are also the most geomorphologically diverse among all the alluvial channel pattern types. Given this diversity, further conceptual research and the development of classification systems covering the entire spectrum of anabranching diversity remain to be explored.

Perhaps some critics can contend that the continuous spectrum of fluvial patterns challenges the effectiveness of a framed four-end-member classification and threshold-based approach, as certain transitional cases may not be adequately categorized. Such concerns often reflect differences between visually based interpretations of channel planforms and quantitative frameworks that rely on systematic metric measurements or comprehensive analyses of processes, landforms, and channel–floodplain relationships. Nonetheless, categorizing river reaches according to prevailing morphologies—anabranching, braided, meandering, or straight—is a scientifically validated methodology. To mitigate uncertainty and avoid classification artefacts, we employed a hierarchical algorithm with quadruple control, grounded in established statistical techniques and methods prominent in previous fluvial geomorphology and large-scale geomorphological research. Our results demonstrate a statistically robust classification; for instance, 85% of total anabranching reaches have an IBI ≥ 1.1, indicating that low thresholds have not skewed outcomes and thereby affirming the validity of the reported global patterns.

A key application of discriminating channel types is their relations with sediment analyses and their interpretation and representativity in the geological record[53–56]. However, reconstructing channel types from the geological records remains challenging due to the limited understanding of the sedimentary structure of contemporary anabranching analogs. Consequently, the recognition of anabranching rivers in the geological record is likely to be significantly underestimated, given the scarce knowledge of the sedimentary signatures of the geomorphological diversity across the spectrum of anabranching channel styles. Another implication of the current dominance of anabranching channels relates to the interaction between vegetation and anabranching patterns throughout the geological record[55], as our results align with the hypothesis of increasing diversification and its dominance of anabranching through the Cenozoic[23].

The diverse interactions between vegetation and channel morphology (sediment trapping, hydraulic effect, banks resistance) in anabranching rivers have been recognized[13,23,57,58]. While some results have explored the hydro-sedimentary and hydro-ecological

connectivity in anabranching rivers, our understanding remains limited. The role of floodplains in hydrochemical and biochemical cycles, sediment transit time, and fluxes of particulate organic carbon oxidation[59,60] is central. Given that the widest and most extensive floodplains (in terms of total global length) are associated with anabranching rivers, the dominance and diversity of these systems have significant implications for biodiversity conservation and the resilience of aquatic ecosystems to climate variability.

Global climate change, driven by warming, is likely to accelerate erosion and sediment supply in cold regions[61], which may result in shifts in river channel patterns. For example, glacier retreat and permafrost melt in mountainous regions could lead to an increase of braided rivers in periglacial zones, while accelerated surface erosion and island migration in large periglacial anabranching rivers, such as Siberia and northern North America[26,62,63], may also occur. Monitoring these shifts and understanding the evolving dynamics of river patterns in response to climate change in those areas are necessary for future river management[28]. As such, it is imperative to integrate perspectives on anabranching systems into ongoing research and management strategies.

Our findings provide substantial insights into fluvial channel patterns, particularly the prevalence of anabranching channels, enhancing our understanding of alluvial channel patterns' spatial characteristics and underlying formation processes. We anticipate that these insights will foster advancements that integrate the unveiled role of anabranching patterns in river science, driving innovations in context-specific fluvial engineering, management, and restoration strategies.

Methods

Data sources

The GSWO dataset[31] served as our primary data source, providing comprehensive and extensive information regarding the location and probability (quantified on a range from 0 to 100%) of historical water occurrences over the past four decades (from 1984 to 2020). It was established using high-resolution 30 m Landsat satellite observations at a global scale spanning a substantial geographical expanse from 60°S to 80°N. By harnessing the GSWO dataset, readily accessible through Google Earth Engine (GEE), we embarked on a comprehensive investigation that sheds light on the extent of global rivers and the classification of different alluvial channel types.

The SWORD[32] was employed as the primary reference for our study of global river networks and their hydrologic attributes. SWORD represents a congruent product amalgamating multiple global hydrography databases to assemble an extensive river network. Its integration includes a wide array of resources such as the Global River Widths from Landsat[64], MERIT Hydro[33], HydroBASINS[65], Global River Obstruction Database[66], Global Delta Maps[67], and HydroFALLS. SWORD hosts a vast collection of 213,485 reaches, each approximately 10 km in length, replete with valuable hydrologic and morphological attributes, including reach average water surface elevation, reach average slope, and reach maximum width, among others.

The GLAKES[68] is a global compilation of lakes derived from the GSWO dataset using a deep-learning model. It delineates the explicit maximum extent of 3.4 million lakes with a surface area greater than 0.03 km^2. Its validation has been corroborated by exceptional accuracy levels, with overall accuracy exceeding 98.7%. In our study, we utilized the GLAKES dataset to precisely ascertain and mask the presence of lakes.

We used the Global Unconsolidated Sediments Map database (GUM)[37] and Global Mountain Biodiversity Assessment (GMBA) Mountain Inventory v2[35,36] to distinguish mountainous and non-mountainous reaches. The GUM provided valuable insights into the distribution of sediments in low relief terrains, an endeavor that incorporated information from 126 individual map sources. It encompassed approximately 50% (68×10^6 km^2) of the global land area (i.e., excluding ice and water bodies), with alluvial sediments covering about 23%, followed by aeolian sediments (21%), glacial sediments (20%), and colluvial sediments (16%). The GMBA Mountains Inventory v2 offered a standardized resource of global mountains with a clear definition based on ruggedness (quantified as highest minus lowest elevation) within eight circular neighborhood analysis windows (NAWs) of different sizes (from 1 pixel to 20 around each point) combined with empirically derived thresholds for each NAW. The GMBA also allowed to complement the identification of non-mountainous regions that are not overlapped by unconsolidated sediments map, such as shields, plateaus, and other hilly areas that are not cataloged as mountains. In addition, we also integrated the deltaic distribution data as identified by Caldwell et al.[34], along with the OpenStreetMap Water Layer (OSMWL) dataset[33], to pinpoint coastal reaches.

The Global Artificial Impervious Areas (GAIA)[69] annual maps provide an extensive record spanning over three decades from 1985 to 2018 at a 30 m resolution, with the mean overall accuracy surpassing 90%. The transition year, from pervious to impervious, can be identified through the pixel values, ranging from 34 (corresponding to 1985) to 1 (indicative of 2018). We leveraged the GAIA to examine whether the islands were overlapped by artificial impervious areas, which comprises any material that impedes or prevents natural water infiltration into the soil.

The hydro-geomorphic factors used to study the complex interactions driving alluvial channel patterns include water surface slope, unit stream power, average floodplain width to average channel width ratio (FPW/W), and suspended sediment concentrations. The global reach-scale ICESat-2 River Surface Slope (IRIS) dataset[70] provides water surface slope derived from ICESat-2 observations. Unit stream power is calculated using bankfull discharge and bankfull width provided by the reach-level bankfull river width dataset[71]. Average floodplain width to average channel width ratio is determined by GSWO dataset using morphological operations and RivWidthCloud algorithm. Global fluvial sediment dataset[72] supplies suspended sediment concentrations for global river reaches. For a detailed calculation of these variables please see Supplementary Note 3 and Supplementary Fig. 1.

Development of an alluvial channel pattern classification algorithm

We generated global maps of alluvial channel patterns using GSWO imagery, with all processing conducted within GEE. The classification workflow is outlined in Supplementary Fig. 1 and involves two key steps: (1) extraction of channel extent from GSWO data; and (2) classification of alluvial channel patterns. The classification step proceeds by (a) distinguishing channels with islands (bars) from those without; (b) differentiating braided and anabranching patterns among islands-bars channels; and (c) identifying straight versus meandering patterns in channels without islands (bars). It is important to note that terms such as braided, meandering, and anabranching apply specifically to alluvial channels and are not appropriate for bedrock-confined rivers, which lack the morphological freedom to develop such planforms. For instance, the Colorado River in Canyonlands National Park incises resistant sedimentary formations, while the Tongtian and Yalu Rivers are constrained by mountainous bedrock valleys (Supplementary Fig. 15a–d). Accordingly, our analysis is limited to alluvial channels, where planform morphology reflects fluvial sediment dynamics rather than structural control.

Our initial step involved delineating the extent of global river channel using the RivWidthCloud algorithm[73,74] to differentiate river pixels from non-river pixels. This distinction was based on binary water extent derived using a threshold of GWSO and river centerlines supplied by the SWORD dataset. Specifically, the GSWO was masked by the OSMWL to exclude ocean pixels and masked by the GLAKES to exclude

instances where reaches encountered the pixels of lakes or reservoirs. To ensure comprehensive coverage of expansive multi-threaded reaches under high-flow and within-bank conditions, we applied a 25% threshold to the GSWO image to generate the binary water extent and exclude intermittent arid channels inundated for less than one season (Supplementary Note 2). Subsequently, buffer zones were created around each SWORD centerline, extending to triple the maximum reach width available via the SWORD dataset to ensure comprehensive coverage[2]. These buffers were used to clip the binary water extent image, following which the RivWidthCloud algorithm was applied to extract the channel extent and channel width. All binary water extent pixels connected to the SWORD centerlines were considered channel extent pixels, effectively excluding isolated water bodies lacking connections to the SWORD centerlines.

To reduce uncertainties in planform classification, we applied a minimum channel width threshold of 150 m for all analyses. Islands and bars are difficult to reliably detect in narrower channels (30–<150 m; corresponding to 1–<5 pixels at 30 m resolution), increasing the risk of misclassification (Supplementary Note 1)[29]. A comparison with manual digitization showed that only 10% of channels with widths of 90–120 m had detectable islands or bars using our automated extraction method. This detection rate improved to 45% for widths of 120–150 m and reached 93% for widths wider than 150 m. Accordingly, we excluded all channels narrower than 150 m from pattern frequency analysis. We also removed reaches associated with lakes, reservoirs, dams, waterfalls, artificial canals, and bedrock-confined valleys. Artificial canals were excluded due to their engineered nature and high human intervention, especially in western Europe and lowland deltas of China. The final analysis encompassed 58,790 alluvial river reaches globally, representing 38% of alluvial reaches in the SWORD dataset, or 58% when excluding intermittent arid reaches (i.e., inundated for less than one season per year or not detected at all by GSWO).

Global alluvial channels exhibit a broad array of planform patterns traditionally divided into straight, meandering, braided, and anabranching (multichannel)[1,6,10,75]. Straight and meandering rivers can typically be distinguished by sinuosity, while anabranching rivers are defined as a system of multiple channels separated by semi-permanent alluvial vegetated islands that divide flows even at bankfull discharge[12,14,22], and braided rivers are characterized by unconsolidated channel separated by ephemeral bars with limited riparian vegetation that can be overtopped at less than bankfull flow[44] (Supplementary Fig. 3).

The primary distinction between straight/meandering and anabranching/braided channels lies in the presence of mid-channel islands or bars. Accordingly, we first identified islands and bars fully enclosed within the channel, excluding those in contact with the channel margin (i.e., lateral and point bars). To minimize noise and ensure robust detection, we applied an area threshold of 0.01 km^2 (equivalent to 11 pixels), discarding any islands or bars below this size (Supplementary Fig. 18).

While using the absolute area of islands and bars offers a practical means of identifying single-threaded channels, it alone proved insufficient to reliably differentiate between straight, meandering, anabranching, and braided channels at the ~10 km reach scale. Transitional or ambiguous morphologies could lead to misclassification. To improve classification accuracy, we introduced an IBI, adapted from the approach of Wang et al.[29]. For each reach containing islands or bars, we generated a bounding circle with a diameter equal to the corresponding SWORD reach length. IBI was defined as the ratio between the total active channel length within this circle and the original SWORD reach length:

$$\mathrm{IBI} = \frac{L_T}{L_R} \tag{1}$$

where L_T is the total channel length of extracted centerlines—derived from the 25% water occurrence maps using the RivWidthCloud algorithm—and L_R is the SWORD reach length. We excluded islands or bars with a surface area <0.3 km^2 to reduce centerline complexity, smoothed the extracted centerlines using the Smooth Line function to eliminate sharp angles, and removed short spurious branches (< 300 m), aligning with Wang et al.[29].

In theory, reaches with IBI > 1 are considered anabranching or braided channels, whereas those with IBI ≤ 1 are considered straight or meandering. However, when short reaches are located solely on islands, the boundary circle may not encompass the full river extent, leading to inaccurate IBI values. To address this, we additionally calculated the relative area (RA) metric for reaches with IBI ≤ 1 to evaluate whether the presence of islands or bars was morphologically meaningful. RA was defined as the ratio of the total area of extracted islands and bars to the total channel area:

$$\mathrm{RA} = \frac{A_{\text{islands and bars}}}{A_{\text{channel}}} \tag{2}$$

This additional filter helped differentiate reaches where minor features might otherwise lead to misclassification. Specifically, reaches with IBI ≤ 1 and RA < 1% were deemed to lack geomorphologically meaningful islands or bars and were subsequently reclassified as straight or meandering, rather than anabranching or braided types.

Some may argue that reaches with IBI values ranging between 1 and 1.1 could be, for an unaware observer that does not measure systematic metrics, prone to be classified as single-channel reaches because of the relatively short length of secondary branches. But we consider that the threshold of IBI > 1, as proposed by Wang et al., together with the complementary use of the RA metric, are useful to identify and classify anabranching reaches even within this lower IBI range (1–1.1). Notably, 85% of the global anabranching reaches have IBI ≥ 1.1 while only 15% of the anabranching population fall within the 1.0–1.1 range, and from those, just 36% are sinuous (i.e., sinuosity ≥ 1.3). Statistics on branching indexes are presented in Supplementary Figs. 8 and 9.

For anabranching and braided channels, the primary diagnostic criterion lies in the dominance of either stable vegetated islands or dynamic sediment bars within the reach. Braided bars are typically unstable, exhibiting substantial shifts in size, position, and morphology between flood events, whereas islands are geomorphologically stable features that persist over years to millennia. These islands often support perennial vegetation, agricultural use, or even permanent human settlement[14,23,76]. The most elementary model of island formation views them as later stages in the geomorphic evolution of fluvial sandbars, wherein vegetation colonization progressively increases surface roughness and reduces inundation frequency, even under bankfull conditions[6,77]. However, the development of islands and branches is not solely the result of avulsion or amalgamation and vegetation colonization of sandbars. Rather, it involves complex erosional and depositional processes within multichannel systems interacting with floodplains shaped by a variety of inherited landforms with diverse morphosedimentary structures[23,78–87]. Vegetated islands allow branches to maintain hydraulic and hydrologic identity, preventing them from acting as a single unified cross-section during floods—even when partially inundated at times[14,23]. The resilience of these features during seasonal floods, often due to cohesive sediment substrates, allows their identification at multiannual scales (Supplementary Fig. 3d, e). In contrast, braided systems are characterized by active beds, with multiple sediment bars exposed at low stages and shallow channels surrounding these bars. These bars do not act as individual branches, and the cross section tends to morpho-hydraulically homogenize during high discharge events. As a result, braided bars

lacking stabilizing vegetation are frequently submerged during floods and undergo rapid morphological change (Supplementary Fig. 3j–l)[21].

Overall, a fundamental distinction between anabranching and braided channels lies in their in-channel features: islands in anabranching systems are typically vegetated and morphologically stable, whereas bars in braided systems tend to be barren and more dynamic[12,44]. A second key difference is that vegetated islands are more resistant to inundation, while sediment bars are more frequently and easily flooded. To quantitatively differentiate these two channel types, we employed two diagnostic metrics: the normalized difference vegetation index (NDVI) and the inundation ratio (IR). NDVI is a widely used proxy for vegetation cover and greenness, computed as:

$$\mathrm{NDVI} = \frac{\mathrm{SR(near\ infrared)} - \mathrm{SR(red)}}{\mathrm{SR(near\ infrared)} + \mathrm{SR(red)}} \tag{3}$$

where SR(λ) is the atmospherically corrected surface reflectance (dimensionless) at a specific Landsat band. We derived NDVI using the full archive of Landsat surface reflectance products from 1984 to 2020, including Landsat-4 TM, Landsat-5 TM, Landsat-7 ETM+, and Landsat-8 OLI, all accessed through the GEE platform. Low-quality observations—such as those affected by clouds, cloud shadows, snow, ice, or radiometric saturation—were excluded using the CFMask quality assurance (QA) flags[88,89]. To characterize long-term vegetation presence, we applied a maximum value composite approach, selecting the highest NDVI value per pixel across all valid observations. The median NDVI value across all extracted island or bar pixels within each reach was then computed to represent the overall vegetation status of in-channel features. To assess the inundation behavior of in-channel features, we defined the IR as:

$$\mathrm{IR} = 1 - \frac{\mathrm{TC_0}}{\mathrm{TC}} \tag{4}$$

where $\mathrm{TC_0}$ is the total number of island and bar pixels with zero water occurrence (i.e., never inundated), and TC is the total number of pixels classified as islands or bars. The term, $\frac{\mathrm{TC_0}}{\mathrm{TC}}$ thus represents the fraction of island and bar area that remain exposed even during the flood season (i.e., where GSWO = 0), relative to the total area of these features exposed during the broader wet season (i.e., GSWO < 25). Consequently, IR serves as a proxy for the degree of inundation, with higher IR values indicating more frequent submergence and lower values suggesting greater geomorphic stability and flood resistance.

To differentiate anabranching from braided channels, we employed a support vector machine (SVM) classifier, a widely used supervised machine learning technique effective for binary classification tasks[90]. The SVM seeks an optimal decision boundary that maximizes the margin between classes while minimizing hinge loss associated with misclassified samples[91]. We used the median NDVI (derived from the maximum value composite) and the IR as classification features, calculated for 2529 representative reaches distributed across diverse environmental and physiographic regions (Supplementary Fig. 2). Of these, 70% were used to train the model and 30% were reserved for testing its performance. Model optimization was conducted using a grid search approach to identify the best-performing hyperparameters. The final model used a radial basis function kernel with a gamma value of 0.8, which controls the influence of individual data points, and a regularization parameter of 0.5 to balance model complexity and accuracy. The classifier was implemented using the Scikit-learn library[92] and achieved a test accuracy of 0.93. We then applied the trained SVM model to all global river reaches containing mid-channel islands or bars, enabling reliable and consistent classification of anabranching versus braided systems based on their vegetation cover and inundation behavior.

The combined use of NDVI and IR effectively captures the contrasting characteristics of anabranching and braided channels. In general, braided bars exhibit low NDVI and high IR values, reflecting sparse vegetation cover and frequent inundation, while anabranching islands tend to show high NDVI and low IR values, indicating greater vegetative stability and resistance to flooding (Supplementary Fig. 2b; located in the upper left and lower right quadrants, respectively). Nonetheless, several important exceptions merit careful consideration. First, anabranching channels with both low NDVI and IR values are commonly found in cold or arid regions, where stable islands are seldom inundated but support only sparse vegetation due to environmental constraints (Supplementary Fig. 3e). Second, although anabranching islands are generally more resistant to inundation, they may still be submerged during rare and high-magnitude flood events. For instance, in some tropical river systems, such as those in the Amazon basin, anabranching islands can experience inundation with return intervals of approximately 40 years, yet remain geomorphologically stable and sustain dense flood-adapted vegetation (e.g., igapó and várzea forests). Third, to minimize misclassification of island inundation caused by human activities—such as aquaculture ponds, which often appear as low NDVI but high IR features in anabranching systems in regions like the Mekong Delta or southern China—we incorporated artificial impervious area data as an additional diagnostic layer. Reaches containing islands intersected by impervious areas were interpreted as anthropogenically stabilized and thus classified as anabranching, recognizing the stabilizing role of human land use. This supplemental step enhances classification accuracy by accounting for both natural and anthropogenic influences on island stability, thereby improving the distinction between anabranching and braided channels.

It is important to note that some reaches exhibited a "mixed pattern", presenting challenges in classification. However, these reaches were categorized as either anabranching-dominant or braided-dominant based on our systematic classification approach, rather than arbitrary criteria. Representative examples of these mixed patterns, observed in Landsat imagery from various reaches, are provided in Supplementary Fig. 4. While these reaches may resemble braided channels due to the presence of extensive channel bars, the identification of multiple stable vegetated islands—not covered by floods—led to their classification as anabranching-dominant. This pattern was evident even in regions with steep slopes, such as Siberia and Alaska, where one particular reach exhibited a much steeper slope of 200 cm $\mathrm{km^{-1}}$, contrasting with other anabranching systems (Supplementary Fig. 4a–f).

For straight and meandering channels, sinuosity—an established morphological index—was used to differentiate these two types, given their distinct morphological differences. Sinuosity was calculated as the ratio of the reach length (i.e., the SWORD reach length) to the valley length (i.e., the straight-line distance between the reach endpoints):

$$\mathrm{Sinuosity} = \frac{L_\mathrm{R}}{L_\mathrm{V}} \tag{5}$$

where L_R is the SWORD reach length and L_V is the valley length. We utilized the sinuosity threshold of 1.3, in line with previous studies[93–95], to distinguish between straight (low sinuosity) and meandering (high sinuosity) channels. Consequently, all the reaches with sinuosity ≥ 1.3, IBI ≤ 1, and RA < 1% were classified as meandering, and those with sinuosity <1.3, IBI ≤ 1, and RA < 1% were classified as straight. These criteria were incorporated into our classification algorithm used to assign channel types globally. To reduce potential misclassification, we examined well-known active meandering hotspots and found that most temporary islands—often forming at meander necks—did not persist as multi-threaded channels in the 40-year GSWO record. Such

short-lived cutoffs therefore, did not result in misclassifying strongly meandering reaches as anabranching.

It is essential to clarify that the term "wandering channels", which refers to a limited number of channels on Earth, was not used in our classification framework. These channels, typically dominated by bedload transport with fluvial bars exposed at low water levels, resemble braided channels but exhibit some sinuosity and occasionally contain islands. Traditionally considered a transitional pattern between braided and meandering channels[96,97], wandering channels were classified in our study based on their specific characteristics. Specifically, sinuous wandering channels without islands (sinuosity ≥ 1.3) were classified as meandering, while bedload-dominated reaches with exposed bars but lacking islands were categorized as braided channels. Reaches containing multiple channels and stable vegetated islands were classified as anabranching channels. Furthermore, we included anastomosing channels within the broader anabranching category. Anastomosing channels, which are characterized by alluvial multichannel systems dominated by vertical accretion and low energy, often surrounded by flood basins, have been described in early sedimentological and geomorphological studies of rivers such as those in Canada[17], the lower Magdalena River[16], and later in Niger and Rhine Rivers[98]. Following these definitions, anastomosing channels are considered a subset of anabranching family in our classification system.

Assessments of the algorithm performance and comparisons with previous channel pattern classifications

We selected 4413 reference reaches over high-resolution (sub-meter) Google Earth images to evaluate the accuracy of our classified channel types. The selection was carried out through a stratified random sampling strategy to ensure representation across different physiographical regions and channel types. The total number of validation samples for anabranching, braided, meandering, and straight reaches were 2153, 225, 1060, and 975, respectively, spanning various regions globally, including non-mountainous (3091 reaches), mountainous (491 reaches) and coastal (831 reaches) regions (see Supplementary Fig. 5a). For each selected reference reaches, we thoroughly examined all available high-resolution historical images during wet season on Google Earth. Comparing these referenced reaches with our results, we achieved an overall accuracy of 88.4% (Supplementary Fig. 5a and Supplementary Table 1).

We further compared the fraction of anabranching rivers with the corresponding values delineated in previous study[29] (Supplementary Fig. 5b). They utilized an anabranching index defined as the total active channel length (i.e., sum of extracted channel centerlines) divided by the SWORD reach length to identify anabranching. Nevertheless, it was constrained to only the top 20 largest river basins, instead of the whole population of alluvial channels in the world. Their calculation of the anabranching fraction, which included bedrock mountainous and coastal reaches, may be less well justified. Rivers flowing through mountain valleys or bedrocks are often geomorphologically constrained and do not develop any channel patterns. Additionally, coastal reaches influenced by waves or tides are shaped by distinct hydro-geomorphological processes. However, to facilitate a more direct comparison with the previous findings, we included all reaches from mountainous, non-mountainous, and coastal regions for the same 18 largest river basins, although we removed certain reaches crossing bedrock, lakes, reservoirs, dams, waterfalls, artificial canals, etc.

When only comparing channel widths ≥ 180 m in the same 18 basins, as studied by Wang et al., the fractions of anabranching reaches in our GACP dataset showed a strong correlation with the previous study. However, our results revealed higher fractions of anabranching channels provided by GACP compared to Wang et al.'s findings in certain basins, such as Irrawaddy, Parana, and Congo (Supplementary Fig. 5b). These discrepancies arose from methodological differences and inherent limitations within either the GACP or otherwise Wang et al. For instance, our analysis excluded reaches crossing bedrock, reservoirs, artificial canals, etc which usually present single-threaded channels. In contrast, the constraints imposed by their anabranching index could potentially cause an overestimation of the anabranching fraction in certain reaches. Because if the total length of active channel (i.e., the sum of extracted channel centerlines) slightly surpasses the length of a SWORD reach but the reach is in fact single-threaded, it will be erroneously classified as anabranching according to their criteria. These factors underline the complexity of accurately characterizing and quantifying channel patterns on a global scale. Overall, both GACP and Wang et al.'s results offer valuable insights into channel patterns, each with its own strengths and limitations. An important difference that distinguishes GACP is its global coverage (60°S–80°N instead of only a few large basins), and a more thorough categorization of channel types (not only single- or multi- threaded, but also subtypes, i.e., anabranching, braided, meandering, straight), long-term channel pattern (four decades), overall accuracy (> 88%), and the distinction of different environments (non-mountain, mountain, and coastal).

Analyzing the patterns of global channels

We analyzed the dominance and distribution of four channel patterns at different scales (i.e., global, physiographical regions, physio-climate zones, continents, and basin levels), and quantified the degree of anabranching coupled with braiding or sinuous-meandering tendencies in these non-mountainous regions.

To characterize the global distribution of four reach types in different physiographical regions, it is key to establish distinct boundaries to separate non-mountainous from mountainous and coastal reaches. Our study concentrates on fluvial reaches with identifiable floodplains from non-mountainous terrains (simply named "non-mountains"), including those in lowlands, low dissected terrains, cratons, plateaus, and hilly regions that are not classified as mountains. Initially, we excluded the bedrock reaches that are only overlapped by the 1 km buffer boundaries of the GMBA Mountains Inventory but not intersected by the GUM dataset. Subsequently, we differentiated coastal reaches (including deltaic reaches) from inland reaches. Coastal reaches exhibit distinct mechanisms of channel pattern formation, as they are influenced not only by fluvial processes but also by the dynamic interactions of waves and tides[99,100]. Most deltas have formed through the action of distributary channels, which may exhibit anabranching characteristics alongside meandering patterns. Therefore, we identified coastal reaches as those spatially intersected with a 25 km buffer zone of global ocean boundaries obtained from the OSMWL dataset and the deltaic polygons delineated by Caldwell et al.[34]. Reaches with an average elevation exceeding 100 m were also excluded from the coastal reaches, following the same method established by previous research[101]. It is worth noting that we retained inland deltas or fans (e.g., the Peace-Athabasca delta) within the category of inland reaches, as these regions were not influenced by coastal processes. Lastly, we divided inland reaches into mountainous and non-mountainous categories. Likewise, a spatial intersection approach was applied to identify mountainous reaches, defined as those intersected with both the GUM dataset and the 1 km buffer boundaries of the GMBA Mountains Inventory. Therefore, the remainder were divided into non-mountainous reaches that were not overlapped by the GMBA Mountains Inventory. It's important to note, however, that not all alluvial reaches we define are located on sedimentary plains due to the unavailability of high-quality datasets, such as the cratonic areas of South America and large parts of Central and Southern Africa, some relatively smooth terrains that do not fall within the boundaries of mountainous areas and unconsolidated sediment. Besides, although some reaches fall within the boundaries of the unconsolidated sediment defined by GUM dataset, they still remain geologically constrained, resulting that rivers do not develop any channel patterns but

rather undergo incision (down-cutting) (e.g., lower reach of the Baram River). Overall, the quantities of non-mountainous, mountainous, and coastal reaches were 40753, 6478, and 11559, respectively.

Physio-climatic conditions were defined by the present (1980–2016) Köppen-Geiger climate classification map[102] (see Supplementary Fig. 7e), and we used it to separated reaches into five climate zones globally. Furthermore, we performed basin-level statistics for non-mountainous anabranching fractions (see Fig. 3) using level-3 boundaries provided by HydroBASIN dataset[103], with particular emphasis on the 20 largest river basins (with rivers exceeding a mean annual discharge of 1000 $m^3 s^{-1}$, as defined for large rivers by Latrubesse[22]). Notably, our study only accounted for exorheic river basins that eventually flow into the sea. For example, rivers such as the Negro, Madeira, or Japurá are usually considered independent rivers and rank among the top 10 largest rivers globally, but they are treated as part of the Amazon basin in our context.

For all non-mountainous anabranching reaches, we calculated the Degree of Anabranching with Braiding or Sinuous-Meandering Tendencies (DABSMT) as follows:

$$\mathrm{DABSMT} = \frac{\sum \mathrm{WO}}{\mathrm{TC}^{*}25} \tag{6}$$

where TC represents the total pixel counts of islands and bars, WO represents the water occurrence on islands and bars, capped at 25 for normalization when the water occurrence exceeds this limit. In essence, this metric serves as a quantifier of channel morphology, where higher DABSMT values (i.e., a greater likelihood of seasonal flooding) signify a pronounced tendency with braiding or sinuous-meandering for anabranching channels, contrasting with lower values (i.e., a less likelihood of seasonal flooding) that indicate completely anabranching (Supplementary Fig. 17).

At first glance, our analysis seems to indicate a potential overestimation of straight reaches, considering that natural processes in alluvial regions rarely result in single straight channel. But, straight alluvial reaches typically occur under certain specific conditions: (a) in steep mountainous rivers constrained by geological factors (e.g., Lancang River, China), or short reaches in piedmont areas influenced by neotectonic movements (e.g., piedmont areas of Jaldhaka and Daina rivers, India[104]), (b) in coastal regions where straight reaches often coincide with single channel systems in remarkably cohesive materials, such as deltas and tidal areas (e.g., Mekong Delta and Ganges-Brahmaputra Delta); (c) in transitional straight reaches connected to two anabranching zones; and (d) in transitional reaches within highly deformed tortuous meandering patterns incised on older alluvium or bedrock. Our data showed that a substantial number of straight channels were connected to anabranching or meandering morphological structures (i.e., scenarios of c and d, see Supplementary Fig. 6). Specifically, globally, we identified 1457 straight reaches (13% of all straight reaches in GACP) connected to anabranching, and 1523 (also 13%) connected to meandering. Mean values, with standard deviations, for scenarios c and d were 10,976 ± 4067 m and 11,472 ± 3853 m, respectively.

Statistical analyses to investigate underlying mechanisms in non-mountainous terrains

The use of empirical and mechanistic discriminators has been instrumental in distinguishing alluvial channel patterns in river systems[1,6,75,105,106]. These discriminators (i.e., slope-discharge approach[6,105,107], sediment load approach[1,8], stream power and grain size[75,108], channel stability[106], etc.) have remarkably contributed to our comprehension of local channel controls, yet understanding the global determinants of alluvial channel patterns remains a formidable challenge due to the complex interplay of various factors and the diversity of river systems[109].

We implemented statistical analyses to identify the major variables that played an important role in influencing the formation of various alluvial channel patterns in non-mountainous regions after removing the straight reaches that were connected to anabranching or meandering morphological structures. Among the selected explanatory variables, namely water surface slope, unit stream power, average floodplain width to average channel width ratio (FPW/W), and suspended sediment concentrations (see Supplementary Note 3), we provided histograms illustrating their distributions in Fig. 4, with additional boxplots displaying the characteristics of slope and bankfull discharge. Note that, a portion of reaches lacked values of certain variables, constituting 36% of non-mountainous reaches. These reaches were excluded from our statistical analysis, ensuring that we were still able to preserve and extract meaningful global patterns, even in the face of missing information. Principal component analysis (PCA) was performed as a trial to disclose differences among the four channel types in compound manner (Supplementary Note 3), which helped us assess the relevance of these variables in controlling alluvial channel patterns (Fig. 4f).

Methodological uncertainty and limitations

Uncertainties and limitations regarding the classification and analysis of fluvial channel patterns are acknowledged. For instance, while the majority of reaches can be classified into distinct categories, certain reaches may exhibit transitional patterns that defy easy classification. This introduces uncertainty in the channel pattern classification, particularly regarding the parameters used and the size thresholds for identifying islands or bars that distinguish straight, meandering, braided, and anabranching channels. To minimize these uncertainties and enhance classification reliability, we implemented a quadruple-control framework comprising the adapted IBI, the ratio of islands/bars area to total channel area, channel sinuosity, and a SVM classifier trained on vegetation (NDVI) and inundation (IR) characteristics. This integrative strategy substantially improves the robustness and accuracy of the global classification of alluvial channel patterns.

For channel pattern analysis, the quality of auxiliary datasets—such as the water occurrence map, mountain map, and unconstrained sediments map—can also introduce potential uncertainties. For example, we excluded rivers with extremely low water occurrence over the past four decades (e.g., water occurrence rarely exceeding 25%, indicating less than one season of inundation) when extracting river extent from the GSWO. This was particularly relevant for ephemeral anabranching channels found in central Australia's desert, leading to an underestimation of anabranching in these regions. However, because the channel pattern analysis was performed only for the reaches defined by our GACP dataset, the impact of this underestimation should be limited. Additionally, extracting smaller bars and islands in narrow reaches, where the width is too small to detect such features from the 30 m GSWO map that led us to study only 38% of alluvial reaches in the SWORD dataset or 58% when excluding intermittent arid reaches, presents another challenge. Nevertheless, higher-resolution images (e.g., Sentinel images) can potentially overcome this limitation.

Despite these challenges, our study offers valuable and original insights into the global distribution of fluvial alluvial channel patterns and deepens our understanding of their spatial characteristics and formation processes. Fundamentally, we mapped the entire population of rivers on Earth, encompassing thousands of different channels. Recognizing the inherent complexity of rivers, we acknowledge that there will be outlier cases; however, these are not quantitatively significant enough to affect the overall results and conclusions.

Data availability

The global alluvial channel pattern (GACP) data in this study have been deposited in the Figshare database under accession code https://

figshare.com/s/db4065c089d798f6177c. The SWORD river network database[33] used in this study can be accessed at https://zenodo.org/record/3898569. The Global Surface Water Occurrence dataset[31] is accessible through the Google Earth Engine at https://earthengine.google.com/. The Global Unconsolidated Sediments Map database (GUM)[37] is available at https://doi.org/10.1594/PANGAEA.884822, and the Global Mountain Biodiversity Assessment (GMBA) Mountain Inventory v2[35] can be accessed at https://www.earthenv.org/mountains. The GLAKES[68] is available through the link https://doi.org/10.5281/zenodo.7016548. The GAIA dataset[69] can be accessed at http://data.ess.tsinghua.edu.cn. Source data are provided with this paper.

Code availability

The Python code developed for the alluvial channel pattern is available via Figshare at https://figshare.com/s/db4065c089d798f6177c.

References

1. Schumm, S. A. Patterns of alluvial rivers. *Annu. Rev. Earth Planet. Sci.* **13**, 5–27 (1985).
2. Wu, Q. et al. Satellites reveal hotspots of global river extent change. *Nat. Commun.* **14**, 1587 (2023).
3. Fryirs, K. A. River sensitivity: a lost foundation concept in fluvial geomorphology. *Earth Surf. Process. Landf.* **42**, 55–70 (2017).
4. Mård, J., Di Baldassarre, G. & Mazzoleni, M. Nighttime light data reveal how flood protection shapes human proximity to rivers. *Sci. Adv.* **4**, eaar5779 (2018).
5. Best, J. Anthropogenic stresses on the world's big rivers. *Nat. Geosci.* **12**, 7–21 (2019).
6. Leopold, L. B. & Wolman, M. G. River channel patterns: braided, meandering, and straight. *U.S. Geol. Surv. Prof. Pap.* **282-B**, 39–85 (1957).
7. Drury, G. Relation of morphology to runoff frequency. In *Water, Soil, and Man* (ed. Chorley, R. J.) 418–430 (Methuen, London, 1969).
8. Schumm, S. A. *The Fluvial System* (New York, Wiley, 1977).
9. Miall, A. D. A review of the braided-river depositional environment. *Earth-Sci. Rev.* **13**, 1–62 (1977).
10. Rust, B. R. A classification of alluvial channel systems. *Canadian Society of Petroleum Geologists Memoir* **5**, 187–198 (1977).
11. Alabyan, A. M. & Chalov, R. S. Types of river channel patterns and their natural controls. *Earth Surf. Process. Landf.* **23**, 467–474 (1998).
12. Nanson, G. C. & Knighton, A. D. Anabranching rivers: their cause, character and classification. *Earth Surf. Process. Landf.* **21**, 217–239 (1996).
13. Tooth, S. & Nanson, G. C. Anabranching rivers on the Northern Plains of arid central Australia. *Geomorphology* **29**, 211–233 (1999).
14. Nanson, G. C. Anabranching and anastomosing rivers. In *Treatise on Geomorphology* (Second Edition) (ed. Shroder, J. F.) **6**, 544–564 (Academic Press, 2022).
15. Brice, J. C. Planform properties of meandering rivers. In River Meandering (ed. Elliott, C. M.) 1–15 (ASCE, 1984).
16. Smith, D. G. & Smith, N. D. Sedimentation in anastomosed river systems; examples from alluvial valleys near Banff, Alberta. *J. Sediment. Res.* **50**, 157–164 (1980).
17. Smith, D. G. Anastomosed fluvial deposits: modern examples from Western Canada. In Modern and Ancient Fluvial Systems (eds Collinson, J. & Lewin, J.) **6**, 155–168 (Blackwell Scientific, 1983).
18. Carson, M. Observations on the meandering-braided river transition, the Canterbury plains, New Zealand: part two. *N.Z. Geographer* **40**, 89–99 (1984).
19. David Knighton, A. & Nanson, G. C. Anastomosis and the continuum of channel pattern. *Earth Surf. Process. Landf.* **18**, 613–625 (1993).
20. Huang, H. Q. & Nanson, G. C. Hydraulic geometry and maximum flow efficiency as products of the principle of least action. *Earth Surf. Process. Landf.* **25**, 1–16 (2000).
21. Huang, H. Q. & Nanson, G. C. Why some alluvial rivers develop an anabranching pattern. *Water Resour. Res.* **43**, W07441 (2007).
22. Latrubesse, E. M. Patterns of anabranching channels: the ultimate end-member adjustment of mega rivers. *Geomorphology* **101**, 130–145 (2008).
23. Latrubesse, E. M. Large rivers, megafans and other Quaternary avulsive fluvial systems: a potential "who's who" in the geological record. *Earth-Sci. Rev.* **146**, 1–30 (2015).
24. Tooth, S., Jansen, J. D., Nanson, G. C., Coulthard, T. J. & Pietsch, T. Riparian vegetation and the late Holocene development of an anabranching river: magela Creek, northern Australia. *Geol. Soc. Am. Bull.* **120**, 1021–1035 (2008).
25. Nyberg, B., Sayre, R. & Luijendijk, E. Increasing seasonal variation in the extent of rivers and lakes from 1984 to 2022. *Hydrol. Earth Syst. Sci.* **28**, 1653–1663 (2024).
26. Gautier, E. et al. Fifty-year dynamics of the Lena River islands (Russia): spatio-temporal pattern of large periglacial anabranching river and influence of climate change. *Sci. Total Environ.* **783**, 147020 (2021).
27. Jarriel, T., Swartz, J. & Passalacqua, P. Global rates and patterns of channel migration in river deltas. *Proc. Natl. Acad. Sci. USA* **118**, e2103178118 (2021).
28. Ielpi, A., Lapôtre, M. G., Finotello, A. & Roy-Léveillée, P. Large sinuous rivers are slowing down in a warming Arctic. *Nat. Clim. Change* **13**, 375–381 (2023).
29. Wang, B. et al. Remote sensing of broad-scale controls on large river anabranching. *Remote Sens. Environ.* **281**, 113243 (2022).
30. Nyberg, B., Henstra, G., Gawthorpe, R. L., Ravnås, R. & Ahokas, J. Global scale analysis on the extent of river channel belts. *Nat. Commun.* **14**, 2163 (2023).
31. Pekel, J.-F., Cottam, A., Gorelick, N. & Belward, A. S. High-resolution mapping of global surface water and its long-term changes. *Nature* **540**, 418–422 (2016).
32. Altenau, E. H. et al. The surface water and ocean topography (SWOT) mission river database (SWORD): a global river network for satellite data products. *Water Resour. Res.* **57**, e2021WR030054 (2021).
33. Yamazaki, D. et al. MERIT Hydro: a high-resolution global hydrography map based on latest topography dataset. *Water Resour. Res.* **55**, 5053–5073 (2019).
34. Caldwell, R. L. et al. A global delta dataset and the environmental variables that predict delta formation on marine coastlines. *Earth Surf. Dyn.* **7**, 773–787 (2019).
35. Snethlage, M. A. et al. A hierarchical inventory of the world's mountains for global comparative mountain science. *Sci. Data* **9**, 149 (2022).
36. Snethlage, M. A. et al. *GMBA Mountain Inventory v2*. GMBA-EarthEnv. https://doi.org/10.48601/earthenv-t9k2-1407 (2022).
37. Börker, J., Hartmann, J., Amann, T. & Romero-Mujalli, G. Terrestrial sediments of the earth: development of a global unconsolidated sediments map database (GUM). *Geochem. Geophys. Geosyst.* **19**, 997–1024 (2018).
38. Montgomery, D. R. & Buffington, J. M. Channel-reach morphology in mountain drainage basins. *Geol. Soc. Am. Bull.* **109**, 596–611 (1997).
39. Wohl, E. E. & Merritt, D. M. Bedrock channel morphology. *Geol. Soc. Am. Bull.* **113**, 1205–1212 (2001).

40. Bujalesky, G. G. Holocene coastal evolution of Tierra del Fuego, Argentina. In *Quaternary of South America and Antarctic Peninsula* (ed. Rabassa, J.) **11**, 247–282 (A.A. Balkema, 1998).
41. Roccati, A., Faccini, F., Luino, F., De Graff, J. V. & Turconi, L. Morphological changes and human impact in the Entella River floodplain (Northern Italy) from the 17th century. *Catena* **182**, 104122 (2019).
42. Horsak, M., Bojková, J., Zahrádková, S., Omesová, M. & Helešic, J. Impact of reservoirs and channelization on lowland river macroinvertebrates: a case study from Central Europe. *Limnologica* **39**, 140–151 (2009).
43. Ciszewski, D. & Czajka, A. Human-induced sedimentation patterns of a channelized lowland river. *Earth Surf. Process. Landf.* **40**, 783–795 (2015).
44. Ashmore, P. Morphology and dynamics of braided rivers. *Treatise Geomorphol.* **9**, 289–312 (2013).
45. Lunt, I. & Bridge, J. Evolution and deposits of a gravelly braid bar, Sagavanirktok River, Alaska. *Sedimentology* **51**, 415–432 (2004).
46. Thorne, C. R. et al. Direct measurements of secondary currents in a meandering sand-bed river. *Nature* **315**, 746–747 (1985).
47. Seminara, G. Meanders. *J. Fluid Mech.* **554**, 271–297 (2006).
48. Constantine, J. A., Dunne, T., Ahmed, J., Legleiter, C. & Lazarus, E. D. Sediment supply as a driver of river meandering and floodplain evolution in the Amazon Basin. *Nat. Geosci.* **7**, 899–903 (2014).
49. Ielpi, A., Lapôtre, M. G., Gibling, M. R. & Boyce, C. K. The impact of vegetation on meandering rivers. *Nat. Rev. Earth Environ.* **3**, 165–178 (2022).
50. Wu, C. et al. Lowland river sinuosity on Earth and Mars set by the pace of meandering and avulsion. *Nat. Geosci.* **16**, 747–753 (2023).
51. Nanson, G. C. & Huang, H. Q. Least action principle, equilibrium states, iterative adjustment and the stability of alluvial channels. *Earth Surf. Process. Landf.* **33**, 923–942 (2008).
52. Kleinhans, M. G., de Haas, T., Lavooi, E. & Makaske, B. Evaluating competing hypotheses for the origin and dynamics of river anastomosis. *Earth Surf. Process. Landf.* **37**, 1337–1351 (2012).
53. Davies, N. S. & Gibling, M. R. Cambrian to Devonian evolution of alluvial systems: the sedimentological impact of the earliest land plants. *Earth-Sci. Rev.* **98**, 171–200 (2010).
54. Long, D. G. F. Architecture and depositional style of fluvial systems before land plants: a comparison of Precambrian, early Paleozoic, and modern river deposits. In *From River to Rock Record.* (eds Davidson, S. K., Leleu, S. & North, C.) **97**, 37–61 (SEPM, 2011).
55. Gibling, M. R. & Davies, N. S. Palaeozoic landscapes shaped by plant evolution. *Nat. Geosci.* **5**, 99–105 (2012).
56. Blum, M., Martin, J., Milliken, K. & Garvin, M. Paleovalley systems: insights from Quaternary analogs and experiments. *Earth-Sci. Rev.* **116**, 128–169 (2013).
57. Jansen, J. D. & Nanson, G. C. Functional relationships between vegetation, channel morphology, and flow efficiency in an alluvial (anabranching) river. *J. Geophys. Res.: Earth Surf.* **115** (2010).
58. Jones, J., Collins, A., Naden, P. & Sear, D. The relationship between fine sediment and macrophytes in rivers. *River Res. Appl.* **28**, 1006–1018 (2012).
59. Repasch, M. et al. Fluvial organic carbon cycling regulated by sediment transit time and mineral protection. *Nat. Geosci.* **14**, 842–848 (2021).
60. Torres, M. A. et al. Model predictions of long-lived storage of organic carbon in river deposits. *Earth Surf. Dyn.* **5**, 711–730 (2017).
61. Zhang, T. et al. Warming-driven erosion and sediment transport in cold regions. *Nat. Rev. Earth Environ.* **3**, 832–851 (2022).
62. Tananaev, N. & Lotsari, E. Defrosting northern catchments: fluvial effects of permafrost degradation. *Earth-Sci. Rev.* **228**, 103996 (2022).
63. Chalov, S. & Prokopeva, K. Sedimentation and erosion patterns of the Lena River anabranching channel. *Water* **14**, 3845 (2022).
64. Allen, G. H. & Pavelsky, T. M. Global extent of rivers and streams. *Science* **361**, 585–588 (2018).
65. Lehner, B. & Grill, G. Global river hydrography and network routing: baseline data and new approaches to study the world's large river systems. *Hydrol. Process.* **27**, 2171–2186 (2013).
66. Whittemore, A. et al. A participatory science approach to expanding instream infrastructure inventories. *Earth's. Future* **8**, e2020EF001558 (2020).
67. Tessler, Z. et al. Profiling risk and sustainability in coastal deltas of the world. *Science* **349**, 638–643 (2015).
68. Pi, X. et al. Mapping global lake dynamics reveals the emerging roles of small lakes. *Nat. Commun.* **13**, 5777 (2022).
69. Gong, P. et al. Annual maps of global artificial impervious area (GAIA) between 1985 and 2018. *Remote Sens. Environ.* **236**, 111510 (2020).
70. Scherer, D., Schwatke, C., Dettmering, D. & Seitz, F. ICESat-2 river surface slope (IRIS): a global reach-scale water surface slope dataset. *Sci. Data* **10**, 359 (2023).
71. Lin, P. et al. Global estimates of reach-level bankfull river width leveraging big data geospatial analysis. *Geophys. Res. Lett.* **47**, e2019GL086405 (2020).
72. Sun, X. et al. Changes in global fluvial sediment concentrations and fluxes between 1985 and 2020. *Nat. Sustain.* **8**, 142–151 (2025).
73. Pavelsky, T. M. & Smith, L. C. RivWidth: a software tool for the calculation of river widths from remotely sensed imagery. *IEEE Geosci. Remote Sens. Lett.* **5**, 70–73 (2008).
74. Yang, X., Pavelsky, T. M., Allen, G. H. & Donchyts, G. RivWidthCloud: an automated Google Earth Engine algorithm for river width extraction from remotely sensed imagery. *IEEE Geosci. Remote Sens. Lett.* **17**, 217–221 (2019).
75. Van den Berg, J. H. Prediction of alluvial channel pattern of perennial rivers. *Geomorphology* **12**, 259–279 (1995).
76. Thorne, C. R., Russell, A. P. & Alam, M. K. *Planform Pattern and Channel Evolution of the Brahmaputra River, Bangladesh*. Vol. **75**, 257–276 (Geological Society, London, Special Publications, 1993).
77. Morón, S., Edmonds, D. & Amos, K. The role of floodplain width and alluvial bar growth as a precursor for the formation of anabranching rivers. *Geomorphology* **278**, 78–90 (2017).
78. Leli, I. T., Stevaux, J. C. & Assine, M. L. Origin, evolution, and sedimentary records of islands in large anabranching tropical rivers: the case of the Upper Paraná River, Brazil. *Geomorphology* **358**, 107118 (2020).
79. Ramonell, C. G., Amsler, M. L. & Toniolo, H. Shifting modes of the Paraná River thalweg in its middle/lower reach. *Zeitschrift für Geomorphologie Supplementband*. **129**, 129–142 (2002).
80. Latrubesse, E. M. & Franzinelli, E. The late Quaternary evolution of the Negro River, Amazon, Brazil: implications for island and floodplain formation in large anabranching tropical systems. *Geomorphology* **70**, 372–397 (2005).
81. Mertes, L. A., Dunne, T. & Martinelli, L. A. Channel-floodplain geomorphology along the Solimões-Amazon river, Brazil. *Geol. Soc. Am. Bull.* **108**, 1089–1107 (1996).
82. Sarma, J. Fluvial process and morphology of the Brahmaputra River in Assam, India. *Geomorphology* **70**, 226–256 (2005).
83. Latrubesse, E. M., Amsler, M. L., de Morais, R. P. & Aquino, S. The geomorphologic response of a large pristine alluvial river to tremendous deforestation in the South American tropics: the case of the Araguaia River. *Geomorphology* **113**, 239–252 (2009).

84. Ashworth, P. J. & Lewin, J. How do big rivers come to be different? *Earth-Sci. Rev.* **114**, 84–107 (2012).
85. Lahiri, S. K. & Sinha, R. Tectonic controls on the morphodynamics of the Brahmaputra River system in the upper Assam valley, India. *Geomorphology* **169**, 74–85 (2012).
86. Lewin, J. & Ashworth, P. J. Defining large river channel patterns: alluvial exchange and plurality. *Geomorphology* **215**, 83–98 (2014).
87. Lewin, J. & Ashworth, P. J. The negative relief of large river floodplains. *Earth-Sci. Rev.* **129**, 1–23 (2014).
88. Zhu, Z. & Woodcock, C. E. Object-based cloud and cloud shadow detection in Landsat imagery. *Remote Sens. Environ.* **118**, 83–94 (2012).
89. Foga, S. et al. Cloud detection algorithm comparison and validation for operational Landsat data products. *Remote Sens. Environ.* **194**, 379–390 (2017).
90. Pal, M. & Mather, P. M. Support vector machines for classification in remote sensing. *Int. J. remote Sens.* **26**, 1007–1011 (2005).
91. Awad, M. & Khanna, R. Support Vector Machines. In *Efficient Learning Machines: Theories, Concepts, and Applications for Engineers and System Designers* 39–66 (Apress, 2015).
92. Pedregosa, F. et al. Scikit-learn: machine learning in Python. *J. Mach. Learn. Res.* **12**, 2825–2830 (2011).
93. Brierley, G. J. & Fryirs, K. A. Geomorphology and River Management: Applications of the River Styles Framework (Blackwell, 2005).
94. Moody-Stuart, M. High-and low-sinuosity stream deposits, with examples from the Devonian of Spitsbergen. *J. Sediment. Res.* **36**, 1102–1117 (1966).
95. Horacio, J. River sinuosity index: geomorphological characterisation (CIREF & Wetlands International European Association, 2014).
96. Church, M. Pattern of instability in a wandering gravel bed channel. In *Modern and Ancient Fluvial Systems* (eds Collinson, J. D. & Lewin, L.) **6**, 169–180 (Blackwell Scientific, 1983).
97. Desloges, J. R. & Church, M. A. Wandering gravel-bed rivers. *Can. Geographer/Le. Géographe Canadien* **33**, 360–364 (1989).
98. Makaske, B. Anastomosing rivers: a review of their classification, origin and sedimentary products. *Earth-Sci. Rev.* **53**, 149–196 (2001).
99. Galloway, W. E. Process framework for describing the morphologic and stratigraphic evolution of deltaic depositional systems. In *Deltas, Models for Exploration* (ed. Broussard, M. L.) 87–98 (Houston Geological Society, 1975).
100. Finotello, A. et al. Three-dimensional flow structures and morphodynamic evolution of microtidal meandering channels. *Water Resour. Res.* **56**, e2020WR027822 (2020).
101. Murray, N. J. et al. The global distribution and trajectory of tidal flats. *Nature* **565**, 222–225 (2019).
102. Beck, H. E. et al. Present and future Köppen-Geiger climate classification maps at 1-km resolution. *Sci. Data* **5**, 1–12 (2018).
103. Lehner, B. & Grill, G. *Hydrobasins: Global Watershed Boundaries And Sub-basin Delineations Derived From Hydrosheds Data At 15 Second Resolution—Technical Documentation Version 1. C.* https://data.hydrosheds.org/file/technical-documentation/HydroBASINS_TechDoc_v1c.pdf (2014).
104. Naskar, R. & Bhattacharya, H. Neotectonic and climatic control on channel evolution in the Himalayan foot-hill, northern West Bengal, India–A case study. *J. Earth Syst. Sci.* **132**, 2 (2022).
105. Eaton, B., Millar, R. G. & Davidson, S. Channel patterns: braided, anabranching, and single-thread. *Geomorphology* **120**, 353–364 (2010).
106. Parker, G. On the cause and characteristic scales of meandering and braiding in rivers. *J. Fluid Mech.* **76**, 457–480 (1976).
107. Lane, E. *A Study of the Shape of Channels Formed by Natural Streams Flowing in Erodible Material. Missouri River Division Sediment Series No. 9*. (US Army Engineer Division, Missouri River, Corps of Engineers, Omaha, NE, 1957).
108. Bledsoe, B. P. & Watson, C. C. Logistic analysis of channel pattern thresholds: meandering, braiding, and incising. *Geomorphology* **38**, 281–300 (2001).
109. Słowik, M. The formation of an anabranching planform in a sandy floodplain by increased flows and sediment load. *Earth Surf. Process. Landf.* **43**, 623–638 (2018).

Acknowledgements

We thank Google Earth Engine for providing the Global Surface Water Occurrence dataset and the data processing resources. L.F. was supported by the National Natural Science Foundation of China (grant nos. 42425604 and 42271322), the National Key Research and Development Program of China (grant no. 2022YFC3201802), the Natural Science Foundation of Guangdong Province (2023B1515120061), and Shenzhen Science and Technology Program (KCXFZ20240903093659003). E.P. was supported by various grants from the Ministry of Education, Singapore, under its Academic Research #Tier 1 [RG142/22], #Tier 1 [2021-T1-001-056], #Tier 2 [MOE-T2EP402A20-0001], #Tier 2 [MOE-T2EP50222-0007], Tier3 Climate Transformation Programme - MOE-MOET32022-0006, NIE AcRF - RI 10/22 EP and the Earth Observatory of Singapore (EOS) via its funding from the National Research Foundation Singapore and the Singapore Ministry of Education under the Research Centres of Excellence.

Author contributions

Q.L.: methodology, data processing and analysis, results interpretation, writing and reviewing. E.P.: conceptualization, methodology, results interpretation, writing and reviewing. E.M.L.: conceptualization, research hypothesis, methodology, results interpretation, writing and reviewing. L.F.: conceptualization, methodology, funding and supervision, results interpretation, writing and reviewing. X.P., H.F., Y.L., A.D.S., D.L., W.Q., C.Z., and P.L. participated in interpreting the results and refining the manuscript.

Competing interests

The authors declare no competing interests.

Additional information

Supplementary information The online version contains supplementary material available at https://doi.org/10.1038/s41467-026-68569-z.

Correspondence and requests for materials should be addressed to Edward Park or Lian Feng.

Peer review information *Nature Communications* thanks Bo Wang, and the other, anonymous, reviewer(s) for their contribution to the peer review of this work. A peer review file is available.